Highly-Cyclable Room-Temperature Black Phosphorene Polymer Electrolyte Composites for Li Metal Batteries

Ramin Rojaee [a], Salvatore Cavallo [a,b], Santosh Mogurampelly [c,d], Bill K. Wheatle [e], Vitaliy Yurkiv [a], Ramasubramonian Deivanayagam [a], Tara Foroozan [a], Md Golam Rasul [a], Soroosh Sharifi-Asl [a], Abhijit H. Phakatkar [a], Meng Cheng [a], Seoung-Bum Son [f], Yayue Pan [a], Farzad Mashayek [a], Venkat Ganesan [e], Reza Shahbazian-Yassar [a,✠]

[a] Mechanical and Industrial Engineering Department, University of Illinois at Chicago, Chicago, Illinois 60607, United States

[b] Department of Energy-DENERG, Politecnico di Torino, Corso Duca degli Abruzzi 24, 10129-Torino, Italy

[c] Institute for Computational Molecular Science (ICMS) and Temple Materials Institute (TMI), Temple University, 1925 North 12th St, Philadelphia, PA 19122, United States

[d] Department of Physics, Indian Institute of Technology Jodhpur, Rajasthan 342037, India

[e] Department of Chemical Engineering, University of Texas at Austin, Austin, Texas 78712, United States

[f] Chemical Sciences and Engineering Division, Argonne National Laboratory, 9700 South Cass Avenue, Lemont, IL 60439, United States

Abstract

In spite of significant interest toward solid-state electrolytes owing to their superior safety in comparison to liquid-based electrolytes, sluggish ion diffusion and high interfacial resistance

✠ Corresponding Author: rsyassar@uic.edu

This is the author manuscript accepted for publication and has undergone full peer review but has not been through the copyediting, typesetting, pagination and proofreading process, which may lead to differences between this version and the Version of Record. Please cite this article as doi: 10.1002/adfm.201910749.

limit their application in durable and high-power density batteries. Here, we report a novel quasi-solid Li^+ ion conductive nanocomposite polymer electrolyte containing black phosphorous (BP) nanosheets. The developed electrolyte was successfully cycled against Li metal (over 550 *h* cycling) at 1 $mA.cm^{-2}$ at room temperature. The cycling overpotential dropped by 75% in comparison to BP-free polymer composite electrolyte indicating lower interfacial resistance at the electrode/electrolyte interfaces. Molecular dynamics (MD) simulations revealed that the coordination number of Li^+ ions around $TFSI^-$ pairs and ethylene oxide (EO) chains decreases at the Li metal/electrolyte interface, which facilitates the Li^+ transport through the polymer host. Density functional theory (DFT) calculations confirmed that the adsorption of the LiTFSI molecules at the BP surface leads to the weakening of N and Li atomic bonding and enhances the dissociation of Li^+ ions. This work offers a new potential mechanism to tune the bulk and interfacial ionic conductivity of solid-state electrolytes that may lead to a new generation of lithium polymer batteries with high ionic conduction kinetics and stable long-life cycling.

Keywords: polymer electrolytes, two-dimensional materials, black phosphorous nanosheets, lithium batteries

1. Introduction

Safe batteries with high energy and power density and long cycle life are strongly desirable to enable a new paradigm in the field of energy storage technologies. For decades, organic-based liquid electrolytes have been the primary choice for commercial Li^+ ion batteries. However, these electrolytes pose significant challenges in high energy density batteries due to flammability, dendritic lithium growth, and parasitic reactions[1–4]. Solid-state electrolytes

offer new opportunities to enable Li metal electrodes as anode due to their high specific capacity of 3.86 $A.h.g^{-1}$ and low electronegative standard potential of -3.04 V [5,6]. Polymer-based solid-state electrolytes are great alternatives for liquid electrolytes that can potentially lead to flexible energy storage devices and provide light-weight battery packs [7–9]. However, low ionic conduction within the bulk polymers and across the electrode-polymer interfaces limits the rate of charge and discharging capabilities in polymer batteries[10,11]. Tremendous efforts have been made in improving the ionic conduction and enhancing the electrochemical performance of the lithium-polymer cells by adjusting chemical composition [12,13], modifying the molecular structures of the polymer backbone [14,15], using hybrid solid/liquid electrolytes [16,17] and alignment of composite polymer electrolytes [18]. However, the slow electrochemical kinetics of solid-state electrolytes still limit their performance in Li-metal batteries (LMBs).

Over the past decade, there have been tremendous efforts to increase the ionic conductivity in polymer electrolytes. Creating composite polymer electrolytes (CPE) by using nanomaterial additives such as Al_2O_3 [19,20], TiO_2 [21,22], SiO_2 [23,24], and carbon nanotubes (CNT) [25] has been shown to be effective in improving the electrochemical performance by changing the crystallinity of the polymer backbone and increasing the dynamics of cations through intersegmental motions among the polymer chains. However, the low bulk ionic conductivity and the sluggish transport of Li^+ ions across the interfaces with electrodes still prove to be limiting factors.

Improvements in the molecular interactions of additives with the host polymer are key to boost the ionic conduction in polymer electrolyte. A recent report by Liu *et al.* [26] have shown that the addition of $Li_{0.33}La_{0.557}TiO_3$ (LLTO) nanowires in polyacrylonitrile (PAN) resulted in facile pathways for Li^+ ion conductivity on the surface of LLTO nanowires through the polymer matrix. In order to maximize the molecular interaction between

nanofillers and the host polymer chains and to alter the strength of Li^+ binding with the neighboring anions, the addition of two-dimensional (2D) materials with the highest surface area offers promising opportunities. Interestingly, the utilization of two-dimensional materials in solid-state electrolytes has been scarce. Wu *et al.* [27] have shown that by adding 0.9 *wt.%* graphene oxide (GO) nanosheets to polyacrylonitrile (PAN) the ionic conductivity can reach 1.1×10^{-4} $S.cm^{-1}$ at 30 ºC, which is one order of magnitude higher than that of the filler-free PAN polymer electrolyte. Yuan *et al.*[28] grafted GO nanosheets into poly(ethylene oxide) (PEO) and reported an ionic conduction as high as 2×10^{-5} $S.cm^{-1}$ at room temperature, but the areal capacity was low (~0.17 $mAh.cm^{-2}$). Ye *et al.* [29] designed a PEO-based composite polymer electrolyte by using ionic liquid-functionalized graphene molecular brushes to achieve 1.5×10^{-4} $S.cm^{-1}$ at 60 °*C*. In another report, Shim *et al.* [30] produced a porous solid electrolyte membrane of poly(vinylidene fluoride-co-hexafluoropropylene) (P(VdF-co-HFP)) with functionalized boron nitride nanoflakes (BNNFs) to increase the uptake of liquid electrolyte. However, the major drawbacks of these polymer composites have been either the lack of room temperature high cycling performance or the utilization of flammable organic liquid electrolytes as one of the main constituents of their composite material.

In this report, we show for the first time that nanosheets of black phosphorous (BP) can induce high ionic conductivity at room-temperature in polymer electrolytes with modest cycling performance against Li metal and conventional cathodes. Recent efforts by the authors and others have shown that BP nanosheets have extraordinary low energy barrier for ion mobility along the [100] direction [31–33]. It was shown that the unique puckered structure of BP nanosheets provides anisotropic ion diffusion in zigzag edge, resulting in a highly selective ionic transport properties [32]. In the present work, it is shown that the incorporation of passivated BP nanosheets can effectively trap the anions, and therefore, reduce the

coordination number of ethylene-oxide (EO) groups and $TFSI^-$ anions around Li^+ ions within the composite polymer electrolyte (CPE). The adsorption of the LiTFSI molecules at the BP surface weakens the bond length of N and Li atoms and, therefore, promotes the dissociation of Li^+ ions from the lithium salt. This work demonstrates that the designed CPE delivers high Li^+ ion conductivity comparable to organic liquid electrolytes. Lower overpotential in these composite electrolytes is correlated to availability of undercoordinated Li^+ ions close to the interface with Li metal. Additionally, the long-term stability of the CPE is improved for over 550 *h* cycling against Li||Li electrodes and demonstrated a great rate performance of up to 3C at room temperature against Li||LFP electrodes.

2. Composite polymer electrolyte synthesis and characterization

The semi-conductive nature of BP nanosheets could be a potential impediment to their use in battery applications [34]. As such, the first step in designing BP nanosheets composite electrolyte is to ensure that these nanosheets are electronically insulating to prevent the short circuit of battery [35,36]. The band gap of BP nanosheets is thickness dependent, and monolayer BP nanosheet has a direct band gap of ca. 2.0 *eV* comparing to bulk BP with the value of ca. 0.34 *eV* [37]. Therefore, different methods to tune the band gap and passivation of BP nanosheets were explored. Ryder *et al.*[38] performed covalent aryl diazonium functionalization of exfoliated BP nanosheets. They have shown that this chemical process forms phosphorus-carbon bonds and produces passivated BP flakes. Controlled passivation of BP nanosheets was also reported in other articles [39–42]. Kuntz *et al.* [43] used high purity O_2 and H_2O to provide site selectivity for oxide and hydroxide formation on basal surface and edge sites of BP nanosheets. Therefore, controlled passivation plays a significant role to keep the integrity of BP nanosheets crystal structure and corresponding properties simultaneously. Ding *et al.* [44] performed molecular dynamic (MD) simulation to study the stable

configurations of BP nanosheets after passivation. They have shown that different arrangements of oxygen atoms and hydroxyl groups on BP can tune the band gap.

In the present work, controlled passivation of BP nanosheets was performed to improve the structural stability of the BP nanosheets upon exposure to other chemical components and increase their corresponding band gap up to 4.3-8.6 *eV* [41,43]. Figure 1(a) and Figure S1 show the transmission electron microscopy (TEM), corresponding EDS spectrum and atomic force microscopy (AFM) images of the exfoliated BP nanosheets demonstrating that the nanosheets of over ca. 200 *nm* in lateral size and thickness of 1-8 nm were achieved. The authors believe that the large effective surface area of the BP additives enhance the interactions with Li salt and increase the Li^+ ions transport. X-ray photon spectroscopy (XPS) was used to study the structural integrity of the BP before and after passivation (Figure 1(b) and 1(c)). The presence of Au and Sn in the overall survey of BP crystal is mainly due to the manufacturing processes which uses Au/Sn alloy and it is not present after the BP is exfoliated [45] (Figure 1(b)). In addition, the Si contamination is also detected in the BP crystal which disappears after the exfoliation. The signal for C is mainly related to the contamination from sample holder and atmosphere. The chemical state of pristine and passivated BP nanosheets was probed with core-level O1s and P2p. The core electron binding energies of phosphorus 2p electrons is shown in Figure 1(c). The results presented in Figure 1(c) indicate a doublet peak at ~128 *eV*, which can be deconvoluted into two binding energy signals $P2p_{3/2}$ and $P2p_{1/2}$ at 127.8 *eV* and 128.6 *eV* in BP crystal respectively. These peaks are respectively shifted to 127.7 *eV* and 128.4 *eV* with the exfoliation of BP, owing to the partial charge accumulation of non-conductive surface. Moreover, O1s signals are centered at 529.7 and 529.4 *eV* in BP crystal and passivated BP spectra in Figure 1(c), respectively. The passivated BP induces an explicit shoulder at 531 *eV,* suggesting the surface oxidation of the BP with multiple bonding states of dangling and bridging oxygen bonds compared to that of bulk crystal. Furthermore, the P2p

doublet of the passivated BP, which is exposed to H_2O oxidant agent, is resembling the 2p peak signals of passivated BP nanosheets and suggests their structural integrity [46,47].

A sample illustration of the synthesis procedure for BP/CPE is shown in Figure 1(d). Ternary polymer electrolyte containing poly(ethylene oxide) (PEO)/ glycol dimethyl ether (TEGDME)/1-Ethyl-2,3-dimethylimidazolium bis(trifluoromethylsulfonyl)imide (EMIM-TFSI) and lithium bis(trifluoromethanesulfonyl)imid (Li-TFSI) as lithium salt and passivated BP nanosheets was developed in this study. Different concentrations of passivated BP nanosheets have been used in the synthesis of nanocomposite polymer electrolyte. The samples are labeled as CPE-0P for polymer with no BP, and CPE-0.05P, CPE-0.1P, CPE-0.5P, CPE-1P, CPE-2P for 0.05, 0.1, 0.5, 1, 2 *wt.%* of passivated BP nanosheets additives, respectively. Elemental mapping of C, F, O, S, and P is shown in Figure 1(e). The composition distribution of carbon (C) atoms primarily arises from the ethylene oxide groups of the polymer backbone. Similarly, the density maps of fluorine (F) and sulfur (S) indicate a uniform distribution of their two sources of the 1-Ethyl-3-methylimidazolium bis(trifluoromethylsulfonyl)imide (EMIM-TFSI) and Lithium bis(trifluoromethanesulfonyl)imide (Li-TFSI) salts. Finally, the phosphorus (P) density map is a result of the passivated BP nanosheets additives and oxygen (O) is a common element in all the electrolyte components which are equally distributed throughout the sample, indicating that the nanocomposite electrolyte is homogenously synthesized.

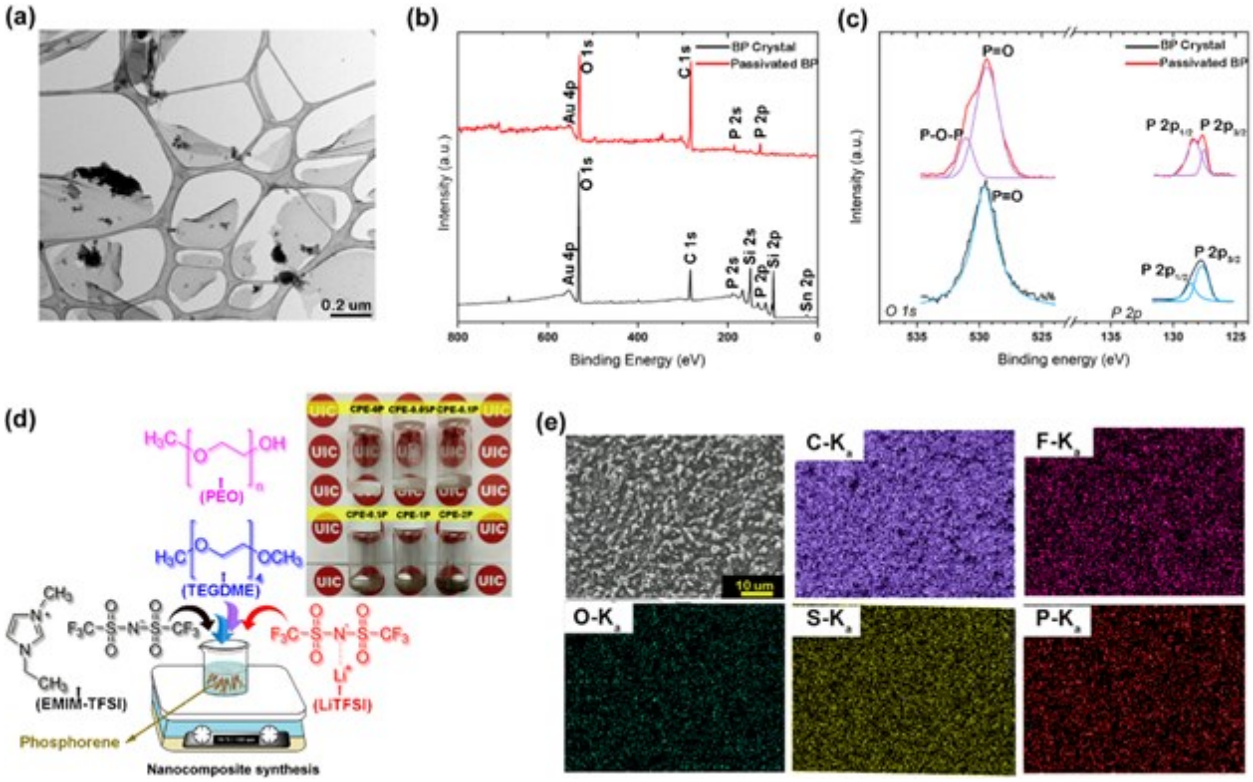

Figure 1. Preparation of the nanocomposite polymer electrolyte with passivated BP nanosheets additive. **(a)** TEM micrograph of the BP nanosheets, (b) Survey XPS spectra and, (c) High-resolution XPS spectra of the P 2p and O 1s signals of the pristine BP crystal and passivated BP nanosheets, (d) Overall synthesis procedure. Inset: Photograph of the developed electrolytes. From left to right: CPE-0P (no additive), and nanocomposite polymer electrolytes with 0.05, 0.1, 0.5, 1, 2 *wt.%* of passivated BP nanosheets, (e) SEM image of the 0.5 *wt.%* with the corresponding EDS mapping.

3. Electrochemical evaluation

The first step was to quantify the optimum concentration of passivated BP nanosheets in the polymer host. Figure S2 shows the ionic conductivity of the CPEs with different concentrations of passivated BP nanosheets. The highest ionic conductivity occurs in CPE-0.5P. Interestingly, the value of the ionic conductivity drops down to 8.1×10^{-4} $S.cm^{-1}$ at 25 ^{o}C upon adding 1 *wt.%* or higher quantity of passivated BP nanosheets into the electrolyte which is likely due to agglomeration of passivated BP nanosheets through the polymer host. This behavior was also observed in other composite electrolytes where optimum amount of organic/inorganic additives are needed to improve the ionic conductivity beyond which the

performance drops [48–50]. In the next section we showed that the rheological behavior of the samples can explain the optimum ionic conductivity due slight increase in shear modulus of the CPE-1P polymer electrolyte. Other possibilities for having an optimum value of ionic conductivity could be possibly due to higher concentration of electrolyte additives. This phenomenon can lead to aggregation of passivated BP nanosheets, resulting excessive number of immobilizing anions. The aggregation behavior of inorganic and organic electrolyte additives has also been reported before [51–54]. For example, Yuan *et al.*[28] developed a PEO-based solid polymer electrolyte with graphene oxide nanosheet additives for Li^+ ion batteries. A significant reduction of tensile strength and ionic conductivity was observed upon adding > 1 *wt.%* of graphene oxide additives. The aggregation of graphene oxide additives was related to be due to their close proximity and high tendency to reduce surface energy [28]. Similar observation was reported by Polu *et al.* [55] who studied the effect of TiO_2 nanoparticles on structural, thermal, mechanical and ionic conductivity of PEO-based solid polymer electrolyte. They showed that when TiO_2 content was increased > 8 *wt.%*, the ionic conductivity decreased from the maximum value. This behavior was attributed to the TiO_2 aggregation and reduction its miscibility in the polymer matrix [55]. While TEM imaging of phosphorene nanosheets distribution in gel polymer electrolytes containing salts and ionic liquid would be challenging due to beam sensitivity, future cryogenic-TEM studies or other imaging techniques can be pursued to study the possible agglomeration of BP in polymer electrolytes at certain concentrations. Therefore, CPE-0.5P was chosen as the optimal concentration of passivated BP nanosheets and was compared to CPE-0.1P as a demonstration of low ion conductivity electrolytes. Both electrolytes were compared to CPE-0P for further electrochemical studies. Figure 2(a) shows the ionic conductivity of the CPE-0P, CPE-0.1P, and CPE-0.5P electrolytes as a function of temperature and their corresponding Nyquist plots at 25 *°C*. Our data analysis pointed out that the ionic

conductivity has increased from 5.9×10^{-4} *S.cm*$^{-1}$ in CPE-0P to 1.2×10^{-3} *S.cm*$^{-1}$ and 2.4×10^{-3} *S.cm*$^{-1}$ in CPE-0.1P and CPE-0.5P composites, respectively. This improvement in ionic conductivity suggests that the addition of passivated BP nanosheets facilitates Li^+ ion transport through the polymeric network during charge/discharge processes. Considering Arrhenius plots in Figure S3, one can measure the activation energy of the Li^+ ions transport through polymer electrolytes [24,56]. Figure S3 demonstrates a deflection in the slope of the graphs. This deflection indicates the phase transformation from solid state to viscous gel [57,58]. Therefore, two values of activation energies (E_a, E'_a) were calculated and summarized in Table S1. As shown in Table S1, activation energy at -5 to 25 *°C* (E_a) decreases from ca. 0.57 *eV* in CPE-0P to ca. 0.42 *eV* after adding BP additives (CPE-0.1P, CPE-0.5P). This indicates that BP additives can effectively lower the activation energy of Li^+ ions transport by ca. 25 *%*. Activation energy is even lower for CPE-0.5P at the temperature range of 35 to 65 *°C* ($E'_{a,CPE\text{-}0.5P} \sim 0.26$ *eV*) rather than CPE-0.1P and CPE-0P with the values of about 0.29 *eV*. The lower activation energy at higher temperature is due to the lower ionic resistance in the electrolyte and the electrode/electrolyte interface. These values are in agreement with other reports [58,59].

Investigation of electrochemical stability window (ESW) of the developed electrolytes provides good information about the oxidative electrochemical stability of electrolytes over a determined voltage range [29]. As shown in Figure 2(b), the onset of change in current appears at about 5 *V* (vs. Li/Li^+) and then a significant peak emerges at about 5.5 *V* (vs. Li/Li^+). This is a clear indication of the oxidative degradation of the polymer network [60,61]. Meaning that, all developed electrolytes have good electrochemical stability up to 5 *V* (vs. Li/Li^+). This is considerably sufficient to guarantee the safe operation of almost all lithium ion battery chemistries. It should be noted that there is a minor current peak starting at about 4.1 *V* vs. Li/Li^+. The electrical current attributed to this behavior is as high as 0.015 *mA* and is about 1

% of the maximum current that occurs at about 5.5 *V* vs. Li/Li^+. This phenomenon could be due to electrolysis of trace humidity in the system which could be trapped into the electrolyte during synthesis and assembly. It is known that water electrolysis occurs at ~+1.23 *V* vs. standard hydrogen electrode (SHE) [62]. Considering that standard electrode potential of Li oxidation/reduction is ~ -3.02 *V* vs. SHE [63], the water electrolysis happens to be ~ +4.25 *V* vs. Li/Li^+ and agrees with our observation. Similar observation was reported at about 4.3-4.6 *V* vs. Li/Li^+, which is ascribed to the electrolysis of remainder of trace trapped humidity in the system [64,65]. This wide ESW allows efficient charge transfer without limiting the cell voltage which allows delivering higher specific energy densities [66–68]. Interestingly, the peak area decreases after adding BP nanosheets. This could be a consequence of less aggressive decomposition reactions which may spike at higher voltages. This observation is in agreement with reports of Xi *et al.* [69] and Hu *et al.* [70] where the addition of mesoporous nanosheets to polymer networks was shown to exhibit excellent electrochemical stability. It is worth noting that ESW of the polymer electrolyte is closely related to chemical and morphological aspects of the host polymer. Armand [71] showed that in general, the limited ESW is due to degradation of polymer chains and decomposition of the anion in the electrolyte. However, the value of ESW is affected by different interactions between the polymer chains, lithium salts and other electrolyte additives [72,73]. Using different Li-salt chemistries, and electrolyte additives can immobilize and electrochemically inactivate the negative charges, which leads to an increased value of electrochemical stability. Zhu *et al.* [52] reported a high ESW of up to 5.4 $V\ vs.\ Li/Li^+$ with PEO@nano-SiO_2 composite polymer electrolyte. This behavior was explained by anions absorption by SiO_2 nanoparticles to decrease their deposition at the cathode side and increasing the polymer oxidation resistance. Similar study has been performed by Park *et al.* [74], which demonstrated that the difference

of surface group arrangements of Al_2O_3 additive to PEO can change the ESW of the composite electrolyte and reach the value of $ca.\ 5\ V\ vs.\ Li/Li^+$.

In order to study the effect of BP nanosheets on the polymer electrolyte in more details, the transference number was measured through electrochemical techniques [75,76]. Transference number shows the fraction of the Li^+ ion motions through the electrolyte in a media containing high concentrations of anions and cations. Therefore, measuring and monitoring this value is a very important factor in developing new electrolytes [77–79]. As shown in Figures S4-S6 and Table S2, the transference number of the polymer composite increases from 0.18 for CPE-0P to 0.32 for CPE-0.5P. Therefore, the incorporation of BP nanosheets can effectively increase the Li^+ ion motion through the electrolyte and improves the electrochemical properties. However, it should be noted that other ionic species may participate in ion conduction properties besides Li^+ ions and limit transference number. However, the authors believe that there is still a room to address this challenge and improve the Li^+ ions transport.

In addition to other electrochemical tests, confirming that the electrical conductivity (EC) is considerably lower compared to ionic conductivity is one of the fundamental requirements of an electrolyte. To confirm that the addition of passivated BP nanosheets does not introduce adverse effects on the insulative nature of the polymer network [35,36], the representative EC plots with polarization voltage of 1 V are displayed in Figure 2(c). Electrical conductivity of the developed electrolytes has been performed by DC polarization tests for the symmetric stainless-steel 316L blocking electrodes. The calculated EC for CPE-0P, CPE-0.1P, and CPE-0.5P recorded as 7×10^{-9}, 3×10^{-9}, and 2×10^{-9} $S.cm^{-1}$. This test was also repeated with 5 mV applied potential to minimize the effect of voltage perturbation to the electrolyte (Figure S7 and Table S3). Both sets of results confirm that the electrical conductivity of the samples

is approximately 10^6 times lower than the ionic conductivity, offering a safe network to transport ions without internal short circuit.

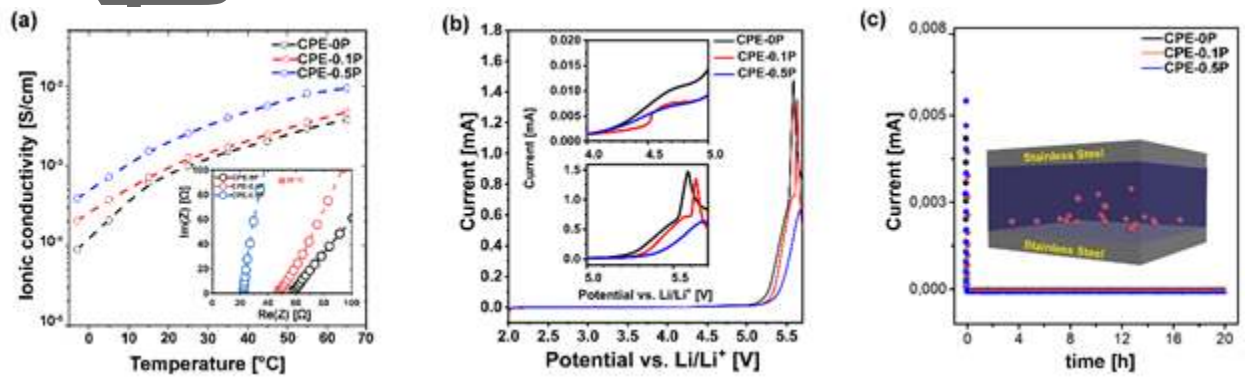

Figure 2- Electrochemical evaluation of the developed electrolytes. (a) Ionic conductivity as a function of temperature for CPE-0P, CPE-0.1P, and CPE-0.5P. The inset graph shows the Nyquist plots corresponding samples at 25 °C, (b) Linear sweep voltammetry showing electrochemical stability window, (c) Direct current polarization tests to measure the electronic conductivity of the developed electrolytes.

Galvanostatic cycling of a battery against symmetric non-blocking electrodes (Li metal) is a preliminary and critical measure in studying the electrochemical capabilities of the developed chemistry of the electrolytes. This test allows studying the overpotential (η) values at different current densities and cycles. The symmetric behavior of the voltage-time profile ensures a homogeneous current distribution on the electrode surface and is a good indication of controlled evolution of solid electrolyte interphase (SEI) layer [80]. This will ultimately result in a higher Coulombic efficiency and longer-life cyclability [81]. The overpotential (η) of a battery is directly proportional to charge transfer resistance at bulk electrolyte (R_{ct}), electrode/electrolyte interfacial resistance ($R_{int.}$) and the applied current (I). This correlation is shown as follows (Equation 1) [17,82];

$$\eta_t = \eta_{ct} + \eta_{int.} = R_{ct} \cdot I + R_{int.} \cdot I \quad (1)$$

where the η_t, η_{ct}, $\eta_{int.}$ and I indicate the total, bulk electrolyte, interface overpotential, and the applied current to the electrochemical cell, respectively. It is well-known that the drastic

changes in overpotential values is a result of non-uniform and unstable solid-electrolyte interphase (SEI) layer that forms on the surface of lithium metal anode upon cycling [4,60]. Usually, as the SEI layer becomes thicker at the electrode/electrolyte interface, the electronic conductance of the electrodes decreases due to its insulating nature [83,84]. Figure 3 shows the voltage profile of the Li||CPE||Li cell configuration at different current densities of 0.05, 0.2, 0.5 and 1 $mA.cm^{-2}$. The average value of overpotential at 0.05 $mA.cm^{-2}$ for CPE-0P ($\eta_{mean,CPE-0P}$) is 120 mV, which is slightly higher than $\eta_{mean,CPE-0.1P}$ and $\eta_{mean,CPE-0.5P}$ (Figure 3(a)). In general, no significant differences can be observed at low current density of 0.05 $mA.cm^{-2}$. However, Figure 3(b) shows that there is a gradual increase in the $\eta_{mean,CPE-0.1P}$ from 200 mV at 150 h to 300 mV at 500 h, suggesting that the resistance of the lithium deposition increases in CPE-0P. Similar behavior was observed for CPE-0.1P, where the $\eta_{mean,CPE-0.5P}$ jumped to 350 mV after 500 h while keeping the symmetric shape of the graph. In contrast, the $\eta_{mean,CPE-0.5P}$ maintained constant value of less than 250 mV in a time period of 500 h at 0.2 $mA.cm^{-2}$, suggesting that the energy barrier of transferring cations across the interface decreases compared to other counterpart electrolytes [82]. Similar but more significant overpotential changes were observed for the higher current densities of 0.5 and 1 $mA.cm^{-2}$. Figures 3(c) and 3(d) display prolonged cycling tests of CPE-0P and CPE-0.5P at current rates of 0.5 and 1 $mA.cm^{-2}$. The $\eta_{mean,CPE-0P}$ at 0.5 $mA.cm^{-2}$ is 430 mV in the initial stages and reaches 280 mV after the 550 h which is higher than that of CPE-0.5P electrolyte with the value of 59 mV. Meanwhile, CPE-0.1P showed a relatively lower voltage polarization values compared to CPE-0P, it reached to 260 mV after 550 h cycling at 0.5 $mA.cm^{-2}$ (Figure 3(c)). $\eta_{mean,CPE-0P}{\sim}915\ mV > \eta_{mean,CPE-0.1P}{\sim}310\ mV > \eta_{mean,CPE-0.5P}{\sim}215\ mV$ at 1 $mA.cm^{-2}$ after 550 cycles was reported in Figure 3(d). This is possibly due to the formation of electrochemically inactive species at the electrode/electrolyte interface and thicker SEI layer

upon long cycling [4,85]. This will change the initial concentration of free cations within the CPE-0P resulting in more drastic changes in overpotential. Overpotential test for CPE-1P at high current density of 1 $mA.cm^{-2}$ was also performed to compare with CPE-0P, CPE-0.1P, and CPE-0.5P. As shown in Figure S8, voltage profile of the CPE-1P shows a fluctuating behavior in a course of 450 *h* and reach to > 1 *V vs.* Li/Li^+ at some time intervals. The average overpotential value of CPE-1P at 1 $mA.cm^{-2}$ over 450 *h* is ~560 *mV* which is higher than the average overpotential value of CPE-0.1P (~310 *mV*), and CPE-0.5P (~120 *mV*) at the same conditions. The authors believe that this behavior is possibly due to the non-uniform distribution of BP at high concentrations thorough composite polymer electrolyte, leading to variable electrochemical interactions of Li^+ ions with the polymer matrix. It is worth noting that the cell cycled at 1 $mA.cm^{-2}$ showed a slightly lower overpotential than the cell cycled at 0.5 $mA.cm^{-2}$ up to about 350 cycles. The cycling tests are possible to undergo some minor changes in different cell assemblies. However, the overpotential values increase more significantly at 1 $mA.cm^{-2}$ after 350 cycles, confirming more aggressive electrochemical conditions at higher current densities and longer cycles. This behavior was further confirmed by studying the interfacial resistance before and after 300 cycles. Figure S9 demonstrate that the total charge transfer resistance value of CPE-0P increased from 746 to 918 $\Omega.cm^{-2}$. Interestingly, the total charge transfer resistance value of CPE-0.5P slightly decreased from 317 to 216 $\Omega.cm^{-2}$ without any parasitic reactions (see Figure S9 and Figure S10). Besides, the rheological tests demonstrate the decrease in viscosity of polymer electrolyte by the addition of BP nanosheets (see detailed explanation in the following section). The decreased viscosity leads to better electrode/electrolyte contact and facilitate the Li^+ ion transport at the interface. In addition, the molecular dynamic simulations that are discussed in this paper further confirm that the BP nanosheets increase the carrier ions (Li^+) at the electrode/electrolyte interface. In addition, no dramatic overpotential deflections were

observed in any sample at any current rates for all samples, indicating that the batteries can be safely used without any short circuit within the tested timeline.

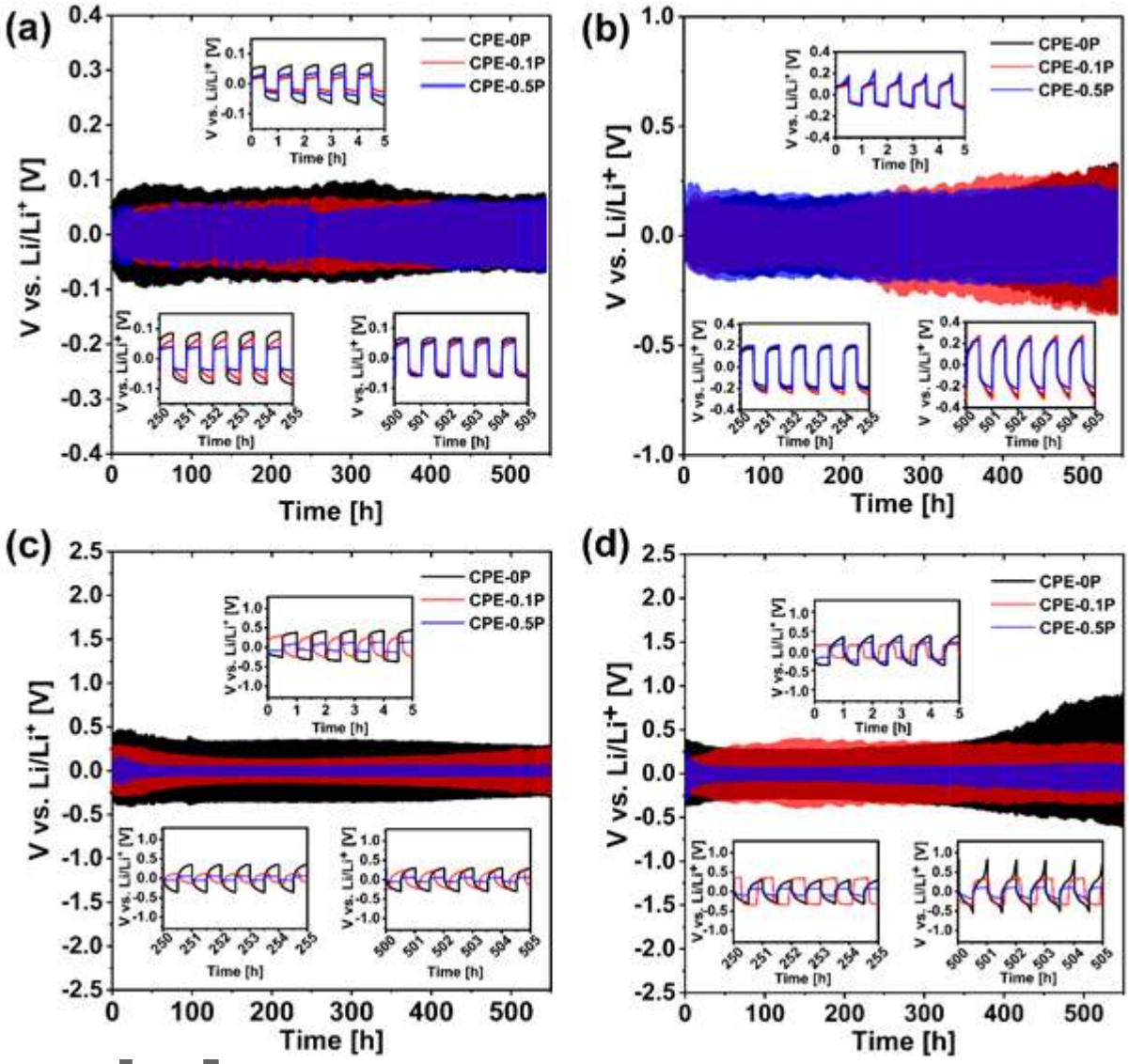

Figure 3. Electrochemical overpotential studies of developed CPEs against Li metal. Time evolution of the potential at various current densities in symmetrical lithium cell (a) 0.05 mA.cm^{-2}, (b) 0.2 mA.cm^{-2}, (c) 0.5 mA.cm^{-2}, and (d) 1 mA.cm^{-2}. Note that the y-axis scale might be different for demonstration purposes.

4. Li^+ ion transport mechanism

To further understand the mechanism of improved electrochemical behavior upon the addition of 2D nanosheets, the association of the ions in polymer backbone was investigated.

As discussed by Rey et al. [86] and Edman [87], FT-IR and Raman vibrational spectra indicate the formation of Li^+-$TFSI^-$ ion clusters and dissociated ions in the range of 730-750 cm^{-1}. The FT-IR and Raman signals consist of two peaks at 740 cm^{-1} and 746 cm^{-1}, which are assigned to the dissociated ions and ion-pairs, respectively in accordance with other reports [88,89]. These peaks are attributed to intramolecular vibrational modes of $TFSI^-$ anions, which implies the transport of Li^+ ions through salt dissociation [89,90]. Since the peaks are normalized with respect to the CH_2-scissoring vibration located in the frequency range 1425-1510 cm^{-1}, the quantification of peaks could be a good indication of the importance of BP additives in the portion of dissociated ions in the electrolyte. More details on peak analysis are provided in the Methods section. As shown in Figures 4(a) and 4(b), upon the addition of passivated BP nanosheets to the polymer electrolyte, the intensity of IR absorbance and Raman signal increase progressively by adding higher concentration of passivated BP nanosheets. To quantify the proportion of intact ion-pairs and dissociated ions, deconvolution analysis has been performed in the same frequency range. According to FT-IR data (inset bar chart in Figure 4(a)), the degree of dissociated Li^+ ions increases from 71% in CPE-0P to 89% and 94% in CPE-0.1P and CPE-0.5P, respectively. The quantification analysis using Raman spectra also confirms the observed enhancements of dissociated ions (Figure 4(a)). The slight differences in the FT-IR and Raman analyses reports could be attributed to the data collection associated with different vibrational modes and energy levels. Overall, the results obtained from FT-IR and Raman experimental measurements confirm that the addition of passivated BP nanosheets results in higher ionic mobility by increasing the ion-pair dissociation in the electrolyte. The full range FTIR and Raman spectra are also provided in Figures S11-S12 for reference.

To examine the ion-pair dissociation mechanism in more detail, nuclear magnetic resonance (NMR) spectroscopy was employed for all the samples to understand the interactions among

Li^+ ions, passivated BP nanosheets and polymer host as shown in Figure 4(c). The ^{7}Li-NMR signal shows a downfield shift of 1.23 ppm for CPE-0P to 1.02 and 0.96 ppm in the presence of passivated BP nanosheets for CPE-0.1P and CPE-0.5P, respectively. This observation is proposed to be due to the changes in the EO-Li^+ and $[(CF_3SO_2)_2N]^- - Li^+$ coordination upon addition of BP nanosheets. This hypothesis is confirmed with MD and DFT simulations later in this paper, which show that the BP nanosheets provide uniform distribution of ionic species through the electrolyte and the electrode/electrolyte interface and entrap the Li^+ ions on the BP surface. This behavior could also be attributed to an increase in the amorphous portion of the polymer host and the anion trapping in the presence of nanofillers [91]. To further understand if the passivated BP nanosheets have any contribution in the degree of crystallinity of the polymer host, differential scanning calorimetry (DSC) was carried out to determine the glass transition temperature (T_g). T_g represents the temperature in which the polymer segments do not have enough energy to rearrange, and therefore, they form a glassy matrix [92,93]. Figure 4(d) shows that the T_g of all the CPE-0P, CPE-0.1P, and CPE-0.5P is ca. -73 °*C* which implies that there is no significant change in crystallinity of the CPEs. Thus, the enhanced ion conduction and outstanding electrochemical properties are not a result of amorphization of the polymer backbone which is a typical explanation of effect of the addition of nanoparticles to polymer matrices [28,91].

Besides the abovementioned mechanism, viscosity is another important factor that could play a critical role in ionic conductivity. The change in viscosity affects the ionic conductivity and diffusion of Li^+ ions through the electrolyte [94]. According to the fractional Walden rule, ionic conductivity and viscosity of the electrolyte are inversely related in PEO-based electrolytes [95,96]. The variation of viscosity of the developed polymer electrolyte at different concentrations of BP additives was studied in Figure S13. As shown in Figure S13, all the samples show near-Newtonian behavior. Interestingly, BP additives decreased the viscosity

in comparison to CPE-0P. This result shows that BP additives lead to segmental motion of polymer chains and facilitate the migration of carrier ions compared to pristine polymer electrolyte [97,98]. In brief, the authors emphasize that the change in viscosity cannot explain the entire behavior of the increase in ionic conductivity since CPE-0.1P and CPE-0.5P both have similar effect on the polymer segmental motions. However, the salt dissociation and immobilizing anions are more sensitive to BP concentration and determine the overall electrochemical behavior.

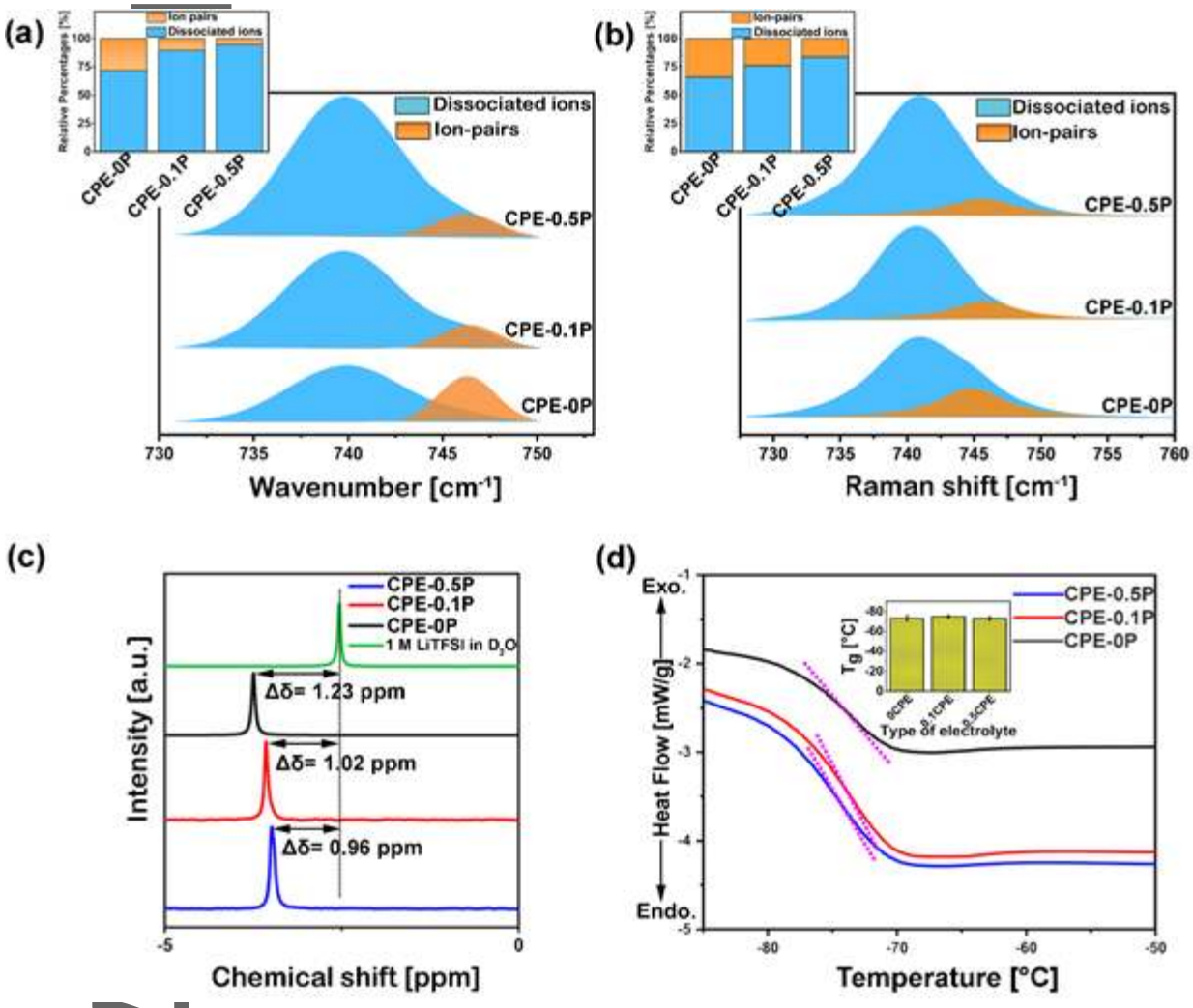

Figure 4- Thermo-chemical characterization of the BP-composite polymer electrolytes. ATR-FTIR (a) and Raman (b) spectra of CPE-0P, CPE-0.1P, CPE-0.5P electrolytes. The inset bar charts quantify these portions for each sample. (c) ^{7}Li NMR spectra.1M LiTFSI in D_2O is used as a control sample. (d) DSC of the composite

polymer electrolytes. The dotted lines and the corresponding bar plot in the inset show the glass transition temperature (T_g).

5. Computational studies: polymer-ion and ion-ion interactions

To support the experimental observations and validate our mechanistic hypotheses, fully atomistic MD simulations of the CPEs were performed to characterize the structure and dynamics of polymers and ions (Figure 5(a)). To characterize the cation-anion association dynamics in the BP-loaded electrolytes, the continuous time auto correlation function *S(τ)* was characterized and are displayed for Li^+-$TFSI^-$ pairs at different temperatures in Figure 5(b). This analysis showed that the Li^+-$TFSI^-$ ion pairs relax more quickly in the BP-loaded electrolytes in comparison to BP-free electrolytes at all temperatures, suggesting lower ion pairing or a higher count of dissociated ions. Similar trend was observed for $EMIM^+$-$TFSI^-$ ion pairs as shown in Figure S16. These findings demonstrate that the addition of passivated BP nanosheets increases the relaxation rate of ion pairing in polymer electrolyte, thereby increasing the experimentally measured conductivity. To further understand the interactions of passivated BP nanosheets with the ion species through the electrolyte, the ratio of anions ($TFSI^-$) to cations (Li^++$EMIM^+$) was studied as a function of distance from a BP nanosheet (Figure 5(c)). As shown in Figure 5(c), $TFSI^-$ ions are present in significantly higher concentrations near (<5 *Å*) the passivated BP nanosheets in comparison to the cations in the system. Thus, it is clear that the addition of BP nanosheets sequesters the $TFSI^-$ anions in the electrolyte, leading to a decrease in ion pairing in agreement with the experimental results of FT-IR and Raman spectra (Figure 4(a,b)).

To study the effect of BP nanosheets on the structural and dynamic properties of the electrolyte and the solvation of Li^+ ion at the Li metal interface, the spatial distribution of Li^+ ion density and the solvation structure near the metal wall interface was examined in Figure 5(d). The normalized Li^+ ion number density (w.r.t. bulk) as a function of the distance from

interface for BP loaded and BP-free electrolytes is presented in Figure 5(e). The density profile of Li^+ ions displays a strong peak in the interfacial zone compared to the bulk system, similar to that reported for a neat PEO-LiTFSI electrolyte [99]. However, the presence of BP nanosheet results in a lower concentration gradient of Li^+ ions near the interface (up to ca. 6 *Å*), thus more uniform distribution of ionic species is expected through the electrolyte and the electrode/electrolyte interface. In general, the aggregation of anions and cations could potentially lead to the formation of a double layer close to the electrode surface. The formation of this double layer can introduce an ionic transport resistance over this boundary layer [99], which is diminished by adding BP nanosheets. Moving away from the interface, Li^+ ion concentration approaches the bulk value for both the BP loaded and BP-free electrolytes ($\rho_{Li^+_{(X)}}/\rho_{Li^+_{bulk}} \rightarrow 1$).

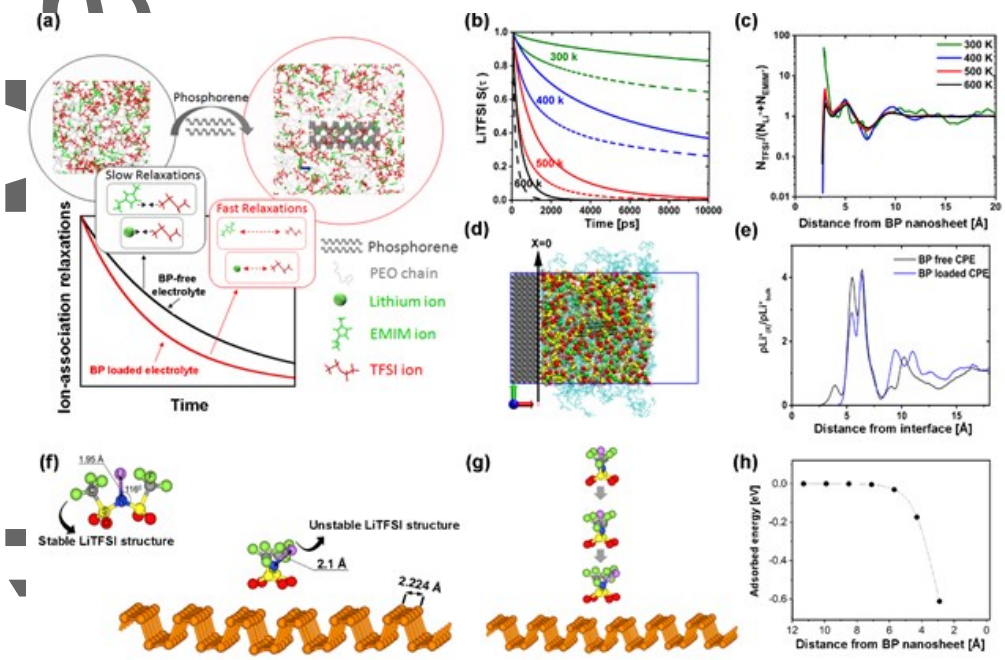

Figure 5. Computational studies of the CPE with BP nanosheets. (a) Schematic of the transport mechanism in bulk electrolyte. (b) The continuous time correlation function for Li^+-$TFSI^-$ ion-pairs. The solid and dashed lines represent BP-free and BP loaded electrolytes respectively. (c) Cumulated number of available $TFSI^-$ ions per cation as a function of the distance away from BP nanosheets. (d) Equilibrated structure of the Li metal/electrolyte interface, (e) Partial density of Li^+ as a function of distance from the

Li metal/electrolyte interface, (f) The most stable configuration of LiTFSI (left) and LiTFSI on the BP (right) as obtained in the present DFT calculations. The adsorption energy is equal to −0.612 eV, and the bond length between the N atom and the Li atom is 2.1 Å, (g) DFT results showing adsorption process of LiTFSI to the BP surface, and (h) the corresponding adsorption energies.

Consistent with the observation on Li^+ ion density profiles, in the interfacial regime (r<10 *Å*), the coordination number of Li^+ ions around $TFSI^-$ ions and EO chains decreases upon addition of passivated BP nanosheets to the electrolyte (Figures S17, S18). This reduction in coordination number indicates that the BP nanosheets promote breaking of ion pairs at the electrode/electrolyte interface and reduce the resistance at this region which is in agreement with our overpotential data (Figure 3).

In order to understand the $Li^+ - TFSI^-$ dissociation mechanism in more detail, the binding energies of LiTFSI to a single BP nanosheet surface were calculated using density functional theory (DFT). The optimized LiTFSI molecule together with the optimized BP nanosheet is shown in Figure S18. Owing to the specific structure of BP nanosheet, there could be several possibilities for LiTFSI adsorption configurations. Figures S19 show results of optimized geometries of LiTSFI adsorbed at BP nanosheet surface. Two possible adsorption geometries were found and named as vertical (Figure S20(a-c)) and horizontal (Figure S20(d,e)) structural configuration of LiTFSI salt near BP nanosheets. The horizontal adsorption structures have more negative adsorption energy than the vertical ones, meaning more stable structure. However, eventually this structure leads to the entrapping of Li^+ ions on the BP surface. The detachment of Li^+ ions from the $TFSI^-$ anion with further insertion between BP arms leads to a very stable P-Li bonding [32]. Considering the present MD and experimental findings, the horizontal configuration will not be considered in this study. In the most stable vertical adsorption, the Li atom moves away from the equilibrium position with increase bond length to 2.1 *Å* comparing to 1.95 *Å* in the equilibrium structure (Figure 5(f)). This

clearly demonstrates that the adsorption of LiTFSI molecule at the BP surface leads to the reduction of interactive force between the N atom and the Li atom, which subsequently leads to dissociation of Li^+ ion.

Following the findings presented in Figure 5(f), the adsorption energies of LiTFSI at different distances away from the BP surface were calculated for most stable vertical configuration (NEB calculations). Figure 5(g) shows the DFT results of this adsorption process depicting atomic structures and corresponding adsorption energies in Figure 5(h). Interestingly, the LiTSFI molecule does not interact with the BP nanosheet surface up to 8 *Å*, where adsorption energy is *ca.* 0 *eV*. However, below 8 *Å* from the surface adsorption energy starts to fall with a visible interaction at 6 *Å*. This is in accordance with our MD simulation which shows a high concentration of anions trap near the BP nanosheets.

6. Cycling performance

Figure 6 shows the capacity-efficiency vs. cycle number of Li||CPE||LFP at constant charge/discharge current density of 140 $mA.g^{-1}$ under a voltage range of 2.5-4.2 *V* vs. Li/Li^+ (Figures 6(a-f)). As demonstrated, the Li||CPE-0P||LFP shows high overpotential value of an average $\eta_{CPE-0P} > 500\ mV$ upon long cycling. In contrast, the voltage hysteresis drops to an average *ca.* 200 *mV* in CPE-0.1P and CPE-0.5P, which corresponds to facilitating the lithiation and de-lithiation processes due to uniform distribution of ionic species at the electrode/electrolyte interface and reducing the ion transport resistance upon the addition of BP nanosheets [12,64]. This observation agrees with our simulation results at electrode/electrolyte interface. Figure S21 summarizes the voltage polarization of the developed electrolytes at different cycles in half-cell Li||LFP cells. Moreover, the CPE exhibits over 90% capacity retention upon the addition of passivated BP nanosheets to the electrolyte that is significantly higher than the CPE-0P with the capacity retention of ca. 30%. This behavior is due to the higher conduction of Li^+ ions in the presence of passivated BP

nanosheets and formation of a protective layer on the electrodes during cycling to avoid parasitic reactions [13,100]. It should be noted that, in the samples with BP additives, the passivation of BP nanosheets may have not been fully performed and very minimal amount of as-synthesized BP nanosheets may have been participated in the side reactions and lowering the Coulombic efficiency slightly. Galvanostatic cycling of Li||CPE||LFP cells was performed at different current densities of 14 $mA.g^{-1}$ and 28 $mA.g^{-1}$ as shown in Figures S22-S23. As can be seen clearly, BP additive improves the electrochemical performance of the CPE by improving the capacity retention. The mean value of Coulombic efficiency remains 99.4% of all the sample types, showing that the developed electrolytes demonstrate good electrochemical stability over 50 cycles. It can be observed that in the sample with no BP additive, the capacity of half-cell Li||CPE-0P||LFP shows a continuous fading trend in all cycling rates. This behavior could be due to high charge transfer resistance resulting in sluggish reactions in the CPE-0P configuration [101,102]. The exact chemistry of sluggish reactions is not known very well and deep chemistry studies are required. However, polymer decomposition may occur at long cycling conditions and lowers the Coulombic efficiency. Additionally, the electrolyte/electrode interface may face a higher resistance over long cycling as discussed earlier, which decreases the ability of the CPE-0P electrolyte to keep a steady capacity at long-term cycles. Although BP nanosheets cannot completely impede the parasitic reactions, the optimum concentration of that can minimize the capacity loss and improve long term performance as can be understood from Figure 6, and Figures S22-S23.

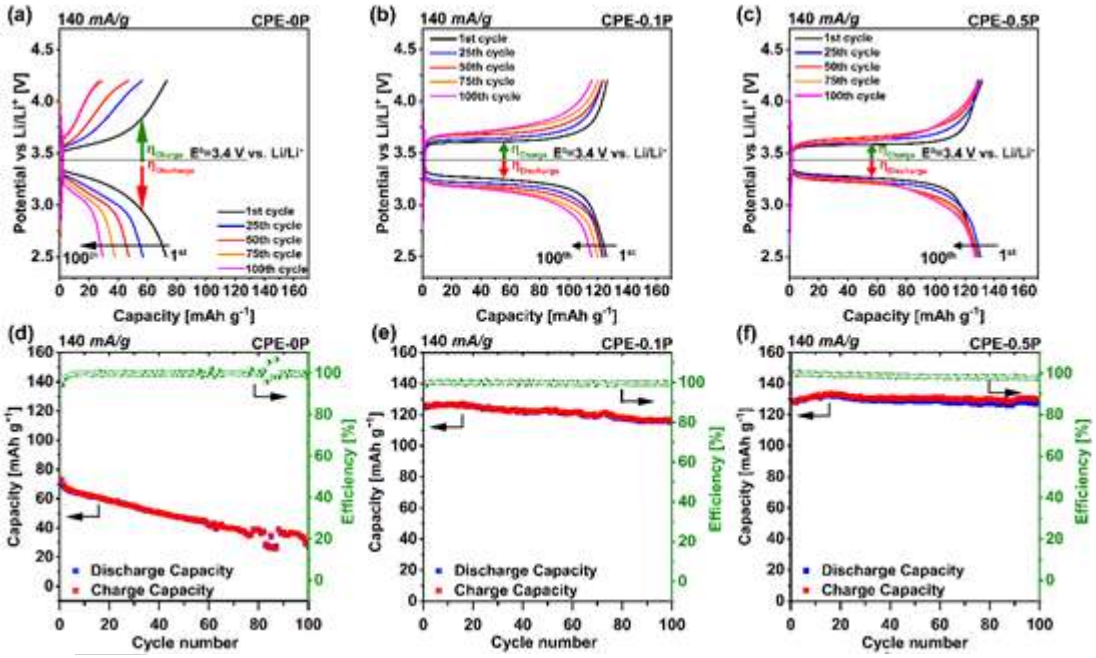

Figure 6- Capacity and efficiency vs. cycle number of the Li||CPE||LFP for developed electrolytes at 140 mA.g^{-1} at 25 °C. Charge–discharge curves of CPE-0P (a), CPE-0.1P (b), CPE-0.5P (c) with different composite additives. The corresponding cycling performance and Coulombic efficiency are displayed in Figures (b), (e), and (f), respectively.

To examine the cyclability of the CPE at different current densities, the rate performance of the electrolytes was monitored (Figure 7). The Li||CPE-0.5P||LFP exhibits good capacity retention at high rate cycling condition. While the CPE-0P sample retains only 10% of the initial capacity at 420 $mA.g^{-1}$, the CPE-0.5P exhibits 80% capacity retention at this current density. This is a clear indication that the BP nanosheets play an important role in boosting the rate performance of batteries. Moreover, in the case of polymer electrolytes containing lower concentration of BP nanosheets (CPE-0.1P), although the capacity reduced to 35-45 $mAh.g^{-1}$ at 420 $mA.g^{-1}$, by decreasing the current density to 14 $mA.g^{-1}$ after 60 cycles, the battery cell retained its initial capacity and cycled very stable. This observation indicates that cycling at high current densities does not damage the electrodes and the poor capacity retention is due to low ionic mobility within the electrolyte. Therefore, passivated BP

nanosheets facilitate Li^+ ion transport and enable the full capacity extraction at high current densities.

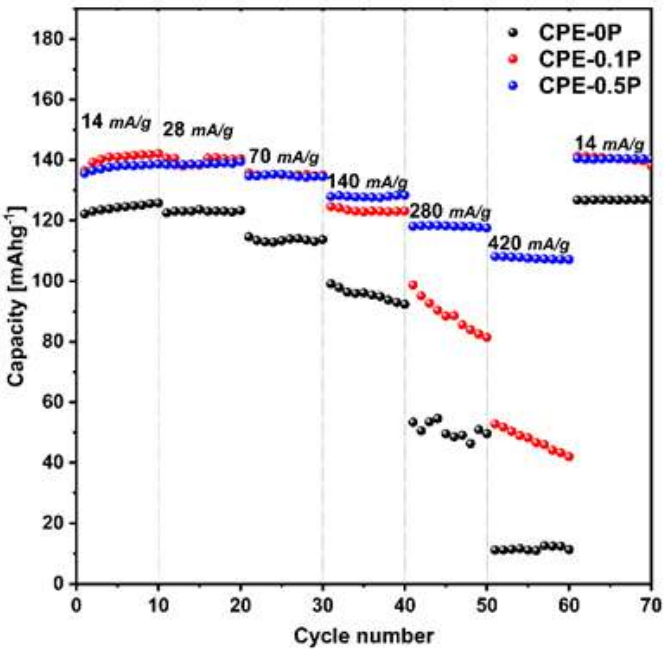

Figure 7- Electrochemical performance of the developed electrolytes at 25 ºC. Rate capability of the CPE-0P, CPE-0.1P, and CPE-0.5P in Li||CPE||LFP cell.

7. Conclusions

In this article, a novel composite polymer electrolyte containing passivated BP nanosheets was designed to achieve one order of magnitude increase in ionic conductivity in comparison to BP-free composites. It was discovered that the passivated BP additives significantly improve the rate cycling stability (up to 420 $mA.g^{-1}$). The addition of 0.5 *wt.%* BP effectively decreases the cycling overpotential values to one-fourth over a prolonged cycling of 550 *h* at 1 $mA.cm^{-2}$. Molecular dynamic studies of Li^+ ion density profiles and coordination numbers in the interfacial zone suggest that adding passivated BP nanosheets results in lowering the tendency of ion-pair formation. Moreover, the BP nanosheets facilitate the Li^+ ion diffusion through bulk electrolyte by aggregating $TFSI^-$ anions and EO groups near their surface. Density functional theory calculations confirmed that the adsorption of the LiTFSI molecule

at the BP surface increases the bond length of N and Li atoms promoting the dissociation of Li^+ ion from Li salt. These new findings provide a novel platform to incorporate 2D materials in design of ion-conductive polymer electrolytes for rechargeable LMBs.

Supporting Information

Supporting Information is available from the Wiley Online Library or from the author.

Acknowledgements

This experimental work is financially supported by the NSF Award number 1620901. The authors acknowledge the characterization facilities provided by University of Illinois at Chicago, Research Resources Center, Electron Microscopy Core and KECK-II facilities of Northwestern University's NU*ANCE* Center. The molecular dynamics simulations reported in this work was funded in part by grants from the Robert A. Welch Foundation (Grant F1599), and the National Science Foundation (CBET-17069698 and DMR-1721512). The authors acknowledge the Texas Advanced Computing Center (TACC) for computing resources. This research also includes calculations carried out on Temple University's HPC resources and thus was supported in part by the NSF through major research instrumentation grant number 1625061 and by the US Army Research Laboratory under contract number W911NF-16-2-0189. We thank Prof. Luciano T. Costa for clarifications on modeling lithium metal wall. The authors acknowledge the financial support from the National Science Foundation award CBET-1805938. In addition, we would like to acknowledge the Advanced Cyberinfrastructure for Education and Research (ACER) group at The University of Illinois at Chicago (URL: https://acer.uic.edu) as well as the National Science Foundation Extreme Science and Engineering Discovery Environment (XSEDE) award no. TG-DMR180106 for providing HPC resources that have contributed to the research results reported in this paper.

Contributions

R.R. and R.S.Y. initiated the idea and designed the experimental protocols. R.R. carried out the electrolyte synthesis, FT-IR, Raman, NMR characterizations of the passivated BP and developed polymer electrolytes. R.R. and S-B. S. performed XPS tests and analysis. R.R. and S.C. carried out the electrochemical measurements and interpretations. R.R. and A.H.P. contributed in BP exfoliation processes A.H.P. performed the TEM imaging. R.R. and M.G.R. performed DSC analysis. Y. P. and M.C. provided the facilities for rheological tests and performed the relevant analyses. S.M., B.K.W., V.G. carried out MD simulation. V.Y. and F.M. performed DFT calculations. The simulation results were discussed and written in collaboration with S.M., B.K.W., V.G., V.Y., F.M., R.R. and R.S.Y. All the authors contributed to the revision and discussion of the manuscript.

References

[1] S. J. An, J. Li, C. Daniel, D. Mohanty, S. Nagpure, D. L. Wood, *Carbon N. Y.* **2016**, *105*, 52.

[2] Q. Li, J. Chen, L. Fan, X. Kong, Y. Lu, *Green Energy Environ.* **2016**, *1*, 18.

[3] J. Mun, T. Yim, J. H. Park, J. H. Ryu, S. Y. Lee, Y. G. Kim, S. M. Oh, *Sci. Rep.* **2015**, *4*, 5802.

[4] T. Foroozan, F. A. Soto, V. Yurkiv, S. Sharifi-Asl, R. Deivanayagam, Z. Huang, R. Rojaee, F. Mashayek, P. B. Balbuena, R. Shahbazian-Yassar, *Adv. Funct. Mater.* **2018**, *28*, 1705917 (1.

[5] K. Kerman, A. Luntz, V. Viswanathan, Y.-M. Chiang, Z. Chen, *J. Electrochem. Soc.* **2017**, *164*, A1731.

[6] J. M. Tarascon, J. M. Tarascon, M. Armand, M. Armand, *Nature* **2001**, *414*, 359.

[7] W. Liu, M.-S. Song, B. Kong, Y. Cui, *Adv. Mater.* **2017**, *29*, 1603436.

[8] L. Long, S. Wang, M. Xiao, Y. Meng, *J. Mater. Chem. A* **2016**, *4*, 10038.

[9] W. H. Meyer, *Adv. Mater.* **1998**, *10*, 439.

[10] P. R. Chinnam, S. L. Wunder, *ACS Energy Lett.* **2017**, *2*, 134.

[11] N. Ohta, K. Takada, L. Zhang, R. Ma, M. Osada, T. Sasaki, *Adv. Mater.* **2006**, *18*, 2226.

[12] I. Osada, H. De Vries, B. Scrosati, S. Passerini, *Angew. Chemie - Int. Ed.* **2016**, *55*, 500.

[13] Y. Zhu, S. Xiao, Y. Shi, Y. Yang, Y. Hou, Y. Wu, *Adv. Energy Mater.* **2014**, *4*, 1.

[14] R. Khurana, J. L. Schaefer, L. A. Archer, G. W. Coates, *J. Am. Chem. Soc.* **2014**, *136*, 7395.

[15] M. Li, W. Zhu, P. Zhang, Y. Chao, Q. He, B. Yang, H. Li, A. Borisevich, S. Dai, *Small* **2016**, 3535.

[16] R. Tan, R. Gao, Y. Zhao, M. Zhang, J. Xu, J. Yang, F. Pan, *ACS Appl. Mater. Interfaces* **2016**, *8*, 31273.

[17] M. R. Busche, T. Drossel, T. Leichtweiss, D. A. Weber, M. Falk, M. Schneider, M. L. Reich, H. Sommer, P. Adelhelm, J. Janek, *Nat. Chem.* **2016**, *8*, 1.

[18] J. Wan, J. Xie, X. Kong, Z. Liu, K. Liu, F. Shi, A. Pei, H. Chen, W. Chen, J. Chen, X. Zhang, L. Zong, J. Wang, L.-Q. Chen, J. Qin, Y. Cui, *Nat. Nanotechnol.* **2019**, *14*, 705.

[19] L. V. N. R. Ganapatibhotla, J. K. Maranas, *Macromolecules* **2014**, *47*, 3625.

[20] S. Das, A. Ghosh, *J. Appl. Phys.* **2015**, *117*, 174103.

[21] M. Hema, P. Tamilselvi, G. Hirankumar, *Ionics (Kiel).* **2017**, *23*, 2707.

[22] C. Ma, J. Zhang, M. Xu, Q. Xia, J. Liu, S. Zhao, L. Chen, A. Pan, D. G. Ivey, W. Wei, *J. Power Sources* **2016**, *317*, 103.

[23] D. Lin, W. Liu, Y. Liu, H. R. Lee, P. C. Hsu, K. Liu, Y. Cui, *Nano Lett.* **2016**, *16*, 459.

[24] N. Zebardastan, M. H. Khanmirzaei, S. Ramesh, K. Ramesh, *Electrochim. Acta* **2016**, *220*, 1.

[25] C. Tang, K. Hackenberg, Q. Fu, P. M. Ajayan, H. Ardebili, *Nano Lett.* **2012**, *12*, 1152.

[26] W. Liu, S. W. Lee, D. Lin, F. Shi, S. Wang, A. D. Sendek, Y. Cui, *Nat. Energy* **2017**, *2*, 1.

[27] B. Wu, L. Wang, Z. Li, M. Zhao, K. Chen, S. Liu, Y. Pu, J. Li, *J. Electrochem. Soc.* **2016**, *163*, A2248.

[28] M. Yuan, J. Erdman, C. Tang, H. Ardebili, *RSC Adv.* **2014**, *4*, 59637.

[29] Y.-S. Ye, H. Wang, S.-G. Bi, Y. Xue, Z.-G. Xue, X.-P. Zhou, X.-L. Xie, Y.-W. Mai, *J. Mater. Chem. A* **2015**, *3*, 18064.

[30] J. Shim, H. J. Kim, B. G. Kim, Y. S. Kim, D.-G. Kim, J.-C. Lee, *Energy Environ. Sci.* **2017**, *10*, 1911.

[31] F. Xia, H. Wang, Y. Jia, *Nat. Commun.* **2014**, *5*, 1.

[32] A. Nie, Y. Cheng, S. Ning, T. Foroozan, P. Yasaei, W. Li, B. Song, Y. Yuan, L. Chen, A. Salehi-Khojin, F. Mashayek, R. Shahbazian-Yassar, *Nano Lett.* **2016**, *16*, 2240.

[33] Y. Cheng, Y. Zhu, Y. Han, Z. Liu, B. Yang, A. Nie, W. Huang, R. Shahbazian-Yassar, F. Mashayek, *Chem. Mater.* **2017**, *29*, 1350.

[34] M. Umar Farooq, A. Hashmi, J. Hong, *Sci. Rep.* **2015**, *5*, 12482.

[35] F. Wu, N. Chen, R. Chen, Q. Zhu, G. Tan, L. Li, *Adv. Sci.* **2015**, 1.

[36] J. Hassoun, R. Verrelli, P. Reale, S. Panero, G. Mariotto, S. Greenbaum, B. Scrosati, *J. Power Sources* **2013**, *229*, 117.

[37] S. Wu, K. S. Hui, K. N. Hui, *Adv. Sci.* **2018**, *5*.

[38] C. R. Ryder, J. D. Wood, S. A. Wells, Y. Yang, D. Jariwala, T. J. Marks, G. C. Schatz, M. C. Hersam, *Nat. Chem.* **2016**, *8*, 597.

[39] V. V. Chaban, E. E. Fileti, O. V. Prezhdo, *ACS Nano* **2017**, *11*, 6459.

[40] M. T. Edmonds, A. Tadich, A. Carvalho, A. Ziletti, K. M. O'Donnell, S. P. Koenig, D. F. Coker, B. Özyilmaz, A. H. C. Neto, M. S. Fuhrer, *ACS Appl. Mater. Interfaces* **2015**, *7*, 14557.

[41] J. Lu, J. Wu, A. Carvalho, A. Ziletti, H. Liu, J. Tan, Y. Chen, A. H. Castro Neto, B. Özyilmaz, C. H. Sow, *ACS Nano* **2015**, *9*, 10411.

[42] A. Ziletti, A. Carvalho, P. E. Trevisanutto, D. K. Campbell, D. F. Coker, A. H. Castro Neto, *Phys. Rev. B* **2015**, *91*, 085407.

[43] K. L. Kuntz, R. A. Wells, J. Hu, T. Yang, B. Dong, H. Guo, A. H. Woomer, D. L. Druffel, A. Alabanza, D. Tománek, S. C. Warren, *ACS Appl. Mater. Interfaces* **2017**, *9*, 9126.

[44] B. Ding, W. Chen, Z. Tang, J. Zhang, *J. Phys. Chem. C* **2016**, *120*, 2149.

[45] A. Ambrosi, Z. Sofer, M. Pumera, *Angew. Chemie Int. Ed.* **2017**, *56*, 10443.

[46] H. Kwon, S. W. Seo, T. G. Kim, E. S. Lee, P. T. Lanh, S. Yang, S. Ryu, J. W. Kim, *ACS Nano* **2016**, *10*, 8723.

[47] J. D. Wood, S. A. Wells, D. Jariwala, K. S. Chen, E. Cho, V. K. Sangwan, X. Liu, L. J. Lauhon, T. J. Marks, M. C. Hersam, *Nano Lett.* **2014**, *14*, 6964.

[48] Y. S. Ye, H. Wang, S. G. Bi, Y. Xue, Z. G. Xue, Y. G. Liao, X. P. Zhou, X. L. Xie, Y. W. Mai, *Carbon N. Y.* **2015**, *86*, 86.

[49] A. Kumar, R. Sharma, M. K. Das, P. Gajbhiye, K. K. Kar, *Electrochim. Acta* **2016**, *215*, 1.

[50] S. Chen, J. Wang, Z. Zhang, L. Wu, L. Yao, Z. Wei, Y. Deng, D. Xie, X. Yao, X. Xu, *J. Power Sources* **2018**, *387*, 72.

[51] D. Kim, X. Liu, B. Yu, S. Mateti, L. A. O'Dell, Q. Rong, Y. Chen, *Adv. Funct. Mater.* **2020**, *1910813*, 1.

[52] Y. Zhu, J. Cao, H. Chen, Q. Yu, B. Li, *J. Mater. Chem. A* **2019**, *7*, 6832.

[53] J. Yu, X. Huang, C. Wu, X. Wu, G. Wang, P. Jiang, *Polymer (Guildf).* **2012**, *53*, 471.

[54] M. Cheng, Y. Jiang, W. Yao, Y. Yuan, R. Deivanayagam, T. Foroozan, Z. Huang, B. Song, R. Rojaee, T. Shokuhfar, Y. Pan, J. Lu, R. Shahbazian-Yassar, *Adv. Mater.* **2018**, *30*, 1800615.

[55] A. R. Polu, H. W. Rhee, *J. Ind. Eng. Chem.* **2016**, *37*, 347.

[56] Z. Osman, M. I. Mohd Ghazali, L. Othman, K. B. Md Isa, *Results Phys.* **2012**, *2*, 1.

[57] Z. Osman, M. I. Mohd Ghazali, L. Othman, K. B. Md Isa, *Results Phys.* **2012**, *2*, 1.

[58] Shalu, S. V.K., S. R.K., *J. Mater. Chem. C* **2015**, *3*, 7305.

[59] A. Arya, A. L. Sharma, *J. Phys. D. Appl. Phys.* **2017**, *50*, 443002.

[60] Q. Lu, Y.-B. He, Q. Yu, B. Li, Y. V. Kaneti, Y. Yao, F. Kang, Q.-H. Yang, *Adv. Mater.* **2017**, *29*, 1604460.

[61] C. Tao, M. Gao, B. Yin, B. Li, Y. Huang, G. Xu, *Electrochim. Acta* **2017**, *257*, 31.

[62] Z. Liu, Y. Huang, Y. Huang, Q. Yang, X. Li, Z. Huang, C. Zhi, *Chem. Soc. Rev.* **2020**, *49*, 180.

[63] R. Huston, J. N. Butler, *J. Phys. Chem.* **1968**, *72*, 4263.

[64] J. Wu, H. Zeng, Q. Shi, X. Li, Q. Xia, Z. Xue, Y. Ye, X. Xie, *J. Power Sources* **2018**, *405*, 7.

[65] Y. Tong, Y. Xu, D. Chen, Y. Xie, L. Chen, M. Que, Y. Hou, *RSC Adv.* **2017**, *7*, 22728.

[66] R. Sahoo, A. Pal, T. Pal, *Chem. Commun.* **2016**, *52*, 13528.

[67] W. Wang, Materials Development for All-Solid-State Battery Electrolytes, University of Michigan, 2017.

[68] G. Tan, F. Wu, C. Zhan, J. Wang, D. Mu, J. Lu, K. Amine, *Nano Lett.* **2016**, *16*, 1960.

[69] J. Xi, X. Qiu, X. Ma, M. Cui, J. Yang, X. Tang, W. Zhu, L. Chen, *Solid State Ionics* **2005**, *176*, 1249.

[70] L. Hu, Z. Tang, Z. Zhang, *J. Power Sources* **2007**, *166*, 226.

[71] M. Armand, *Solid State Ionics* **1983**, *9–10*, 745.

[72] L. Chen, S. Venkatram, C. Kim, R. Batra, A. Chandrasekaran, R. Ramprasad, *Chem. Mater.* **2019**, *31*, 4598.

[73] F. Croce, L. L. Persi, B. Scrosati, F. Serraino-Fiory, E. Plichta, M. A. Hendrickson, *Electrochim. Acta* **2001**, *46*, 2457.

[74] C. H. Park, D. W. Kim, J. Prakash, Y. K. Sun, *Solid State Ionics* **2003**, *159*, 111.

[75] J. Evans, C. A. Vincent, P. G. Bruce, *Polymer (Guildf).* **1987**, *28*, 2324.

[76] S. Zugmann, M. Fleischmann, M. Amereller, R. M. Gschwind, H. D. Wiemhöfer, H. J. Gores, *Electrochim. Acta* **2011**, *56*, 3926.

[77] K. D. Fong, J. Self, K. M. Diederichsen, B. M. Wood, B. D. McCloskey, K. A. Persson, *ACS Cent. Sci.* **2019**, *5*, 1250.

[78] M. Chintapalli, K. Timachova, K. R. Olson, S. J. Mecham, D. Devaux, J. M. Desimone, N. P. Balsara, *Macromolecules* **2016**, *49*, 3508.

[79] D. M. Pesko, K. Timachova, R. Bhattacharya, M. C. Smith, I. Villaluenga, J. Newman, N. P. Balsara, *J. Electrochem. Soc.* **2017**, *164*, E3569.

[80] K. N. Wood, M. Noked, N. P. Dasgupta, *ACS Energy Lett.* **2017**, *2*, 664.

[81] A. Wang, S. Kadam, H. Li, S. Shi, Y. Qi, *npj Comput. Mater.* **2018**, *4*, 15 (1.

[82] M. Todd, R. D. Armstrong, In *Solid State Electrochemistry (Chemistry of Solid State Materials)*; Bruce, P. G., Ed.; Cambridge University Press, 1997; pp. 264–291.

[83] E. Peled, *J. Electrochem. Soc.* **1979**, *126*, 2047.

[84] F. S. Li, Y. S. Wu, J. Chou, M. Winter, N. L. Wu, *Adv. Mater.* **2014**, *27*, 130.

[85] D. Lv, Y. Shao, T. Lozano, W. D. Bennett, G. L. Graff, B. Polzin, J. Zhang, M. H. Engelhard, N. T. Saenz, W. A. Henderson, P. Bhattacharya, J. Liu, J. Xiao, *Adv. Energy Mater.* **2015**, *5*, 1.

[86] I. Rey, P. Johansson, J. Lindgren, J. C. Lassègues, J. Grondin, L. Servant, *J. Phys. Chem. A* **1998**, *102*, 3249.

[87] L. Edman, *J. Phys. Chem. B* **2000**, *104*, 7254.

[88] J.-C. Lassègues, J. Grondin, D. Talaga, *Phys. Chem. Chem. Phys.* **2006**, *8*, 5629.

[89] I. Rey, J. C. Lassègues, J. Grondin, L. Servant, *Electrochim. Acta* **1998**, *43*, 1505.

[90] M. Ulaganathan, C. M. Mathew, S. Rajendran, *Electrochim. Acta* **2013**, *93*, 230.

[91] S. Mogurampelly, O. Borodin, V. Ganesan, *Annu. Rev. Chem. Biomol. Eng* **2016**, *7*, 349.

[92] M. Suchitra, In *Advanced Topics in Characterization of Composites*; Kessler, M. R., Ed.; Trafford Publishing, 2004; pp. 11–33.

[93] J. Bicerano, *Prediction of Polymers, Third Edition , Revised and Expanded*; 2002.

[94] C. Comminges, R. Barhdadi, M. Laurent, M. Troupel, *J. Chem. Eng. Data* **2006**, *51*, 680.

[95] M. P. Longinotti, H. R. Corti, *J. Phys. Chem. B* **2009**, *113*, 5500.

[96] D. Bresser, S. Lyonnard, C. Iojoiu, L. Picard, S. Passerini, *Mol. Syst. Des. Eng.* **2019**, *4*, 779.

[97] N. Hasan, M. Pulst, M. H. Samiullah, J. Kressler, *J. Polym. Sci. Part B Polym. Phys.* **2019**, *57*, 21.

[98] H. Sasabe, S. Saito, *Polym. J.* **1972**, *3*, 624.

[99] M. Ebadi, L. T. Costa, C. M. Araujo, D. Brandell, *Electrochim. Acta* **2017**, *234*, 43.

[100] S. M. Eo, E. Cha, D. W. Kim, *J. Power Sources* **2009**, *189*, 766.

[101] Z. Ogumi, *Electrochemistry* **2010**, *78*, 319.

[102] H. Zhang, C. Li, M. Piszcz, E. Coya, T. Rojo, L. M. Rodriguez-Martinez, M. Armand, Z. Zhou, *Chem. Soc. Rev.* **2017**, *46*, 797.

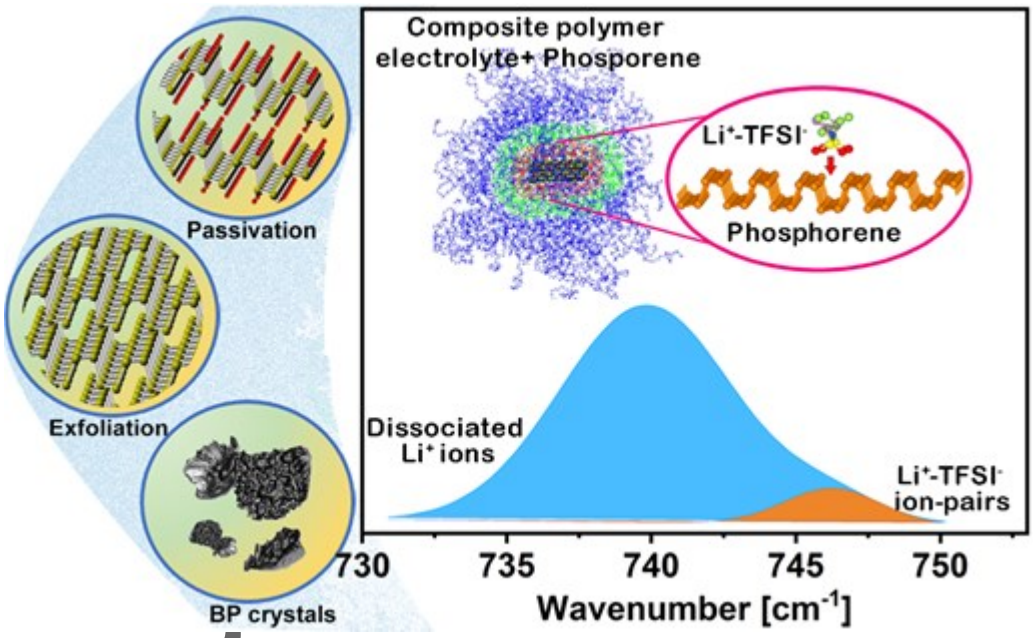

The incorporation of phosphorene (BP) nanosheets effectively increased the Li^+ ion motion through the electrolyte and improved the electrochemical properties. The computer simulation models demonstrated a high concentration of anions trap near the BP nanosheets. This shows a great potential for developing new generation of lithium polymer batteries with high ionic conduction kinetics and stable long-life cycling.